Title

Generic Process for Highly Stable Metallic Nanoparticle-Semiconductor Heterostructures via Click Chemistry for Electro/Photocatalytic Applications

Journal

ACS Applied Materials & Interfaces, 5(19)

ISSN

1944-8244

Authors

Upadhyay, Arun Prakash
Behara, Dilip Kumar
Sharma, Gyan Prakash
et al.

Publication Date

2013-10-09

DOI

10.1021/am402398h

ACS APPLIED MATERIALS & INTERFACES

Research Article

www.acsami.org

Generic Process for Highly Stable Metallic Nanoparticle-Semiconductor Heterostructures via Click Chemistry for Electro/Photocatalytic Applications

Arun Prakash Upadhyay,[†] Dilip Kumar Behara,[†] Gyan Prakash Sharma,[†] Anshumaan Bajpai,[†] Nicholas Sharac,[‡] Regina Ragan,*[,‡] Raj Ganesh S Pala,*[,†] and Sri Sivakumar*[,†,§]

[†]Department of Chemical Engineering, Indian Institute of Technology Kanpur, Kanpur, Uttar Pradesh 208016, India

[‡]Chemical Engineering and Materials Science, University of California—Irvine, Irvine, California 92697-2575, United States

[§]Material Science Programme, Centre for Environmental Science & Engineering, Indian Institute of Technology Kanpur, Kanpur, Uttar Pradesh 208016, India

Supporting Information

ABSTRACT: Metallic nanoparticles (MNP) are utilized as electrocatalysts, cocatalysts, and photon absorbers in heterostructures that harvest solar energy. In such systems, the interface formed should be stable over a wide range of pH values and electrolytes. Many current nonthermal processing strategies rely on physical interactions to bind the MNP to the semiconductor. In this work, we demonstrate a generic chemical approach for fabricating highly stable electrochemically/photocatalytically active monolayers and tailored multilayered nanoparticle structures using azide/alkyne-modified Au, TiO_2, and SiO_2 nanoparticles on alkyne/azide-modified silicon, indium tin oxide, titania, stainless steel, and glass substrates via click chemistry. The stability, electrical, electrochemical, and photocatalytic properties of the interface are shown via electrochemical water splitting, methanol oxidation, and photocatalytic degradation of Rhodamine B (RhB) dye. The results suggest that the proposed approach can be extended for the large-scale fabrication of highly stable heterostructure materials for electrochemical and photoelectrocatalytic devices.

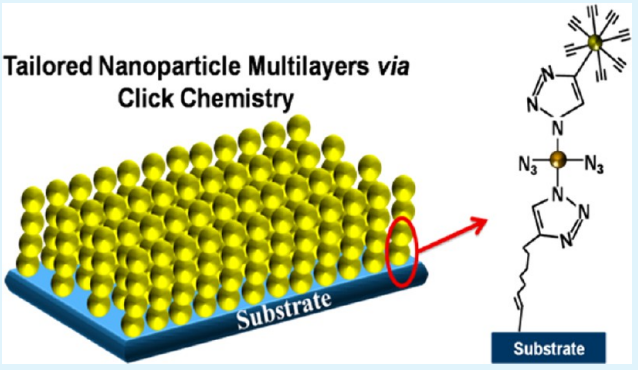

KEYWORDS: *water splitting, heterostructures, layer-by-layer, click chemistry, tailored mono/multilayers, methanol oxidation*

INTRODUCTION

A sustainable approach to large-area solar-energy devices relies on two qualitatively different approaches, namely, high-cost and high-efficiency devices or relatively lower-cost and lower-efficiency devices. Central to the latter approach is the utilization of liquid-phase processing methods that do not rely on single-crystal substrates, thin films, or vacuum fabrication techniques. A chemical approach can harvest solar energy by performing an endothermic reaction; the resulting products can be used as solar-produced chemicals or fuels. Different chemical reactions, such as water splitting,[1−5] oxidation reactions[6−8] and CO_2 conversion,[8,9] are being explored using these methods. Semiconductors play a central role in such devices, and there have been many efforts to improve the photocatalytic efficiency of semiconductors, including bandgap tuning to increase photon absorption cross sections,[1,10−12] adding sensitizers to enhance charge carrier lifetimes by decreasing electron-hole separation,[13−17] and adding cocatalysts to improve surface redox reaction rates.[3,18−20]

Recently, metal-semiconductor heterostructures have gained considerable attention because the incorporation of noble metals (such as Au and Ag) on semiconductors surfaces offered new prospects for enhancing photocatalytic activity as a result of the surface plasmon resonance (SPR) effect of noble metals.[13−16,21−23] However, most metallic-semiconductor heterostructures are fabricated through physical mixing,[15,16] electrochemical deposition,[21] noncovalent interactions,[24−29] spin coating,[30] Langmuir Blodgett,[31] Doctor Blade,[32] and sputtering.[33] However, these heterostructures are stable only under certain chemical conditions because of the relatively weak interactions between the metal and semiconductor surfaces; it is thus expected that covalently bound interfaces would enhance the stability of such heterostructures. Here, we demonstrate a versatile approach to enhance the stability of metallic-semiconductor heterostructures via click chemistry. The

Received: June 20, 2013
Accepted: September 9, 2013
Published: September 9, 2013

Scheme 1. Schematic Representation of the Fabrication of an Azide-Functionalized Nanoparticle Assembly on Alkyne-Functionalized Substrates via Click Chemistry (Surface A)

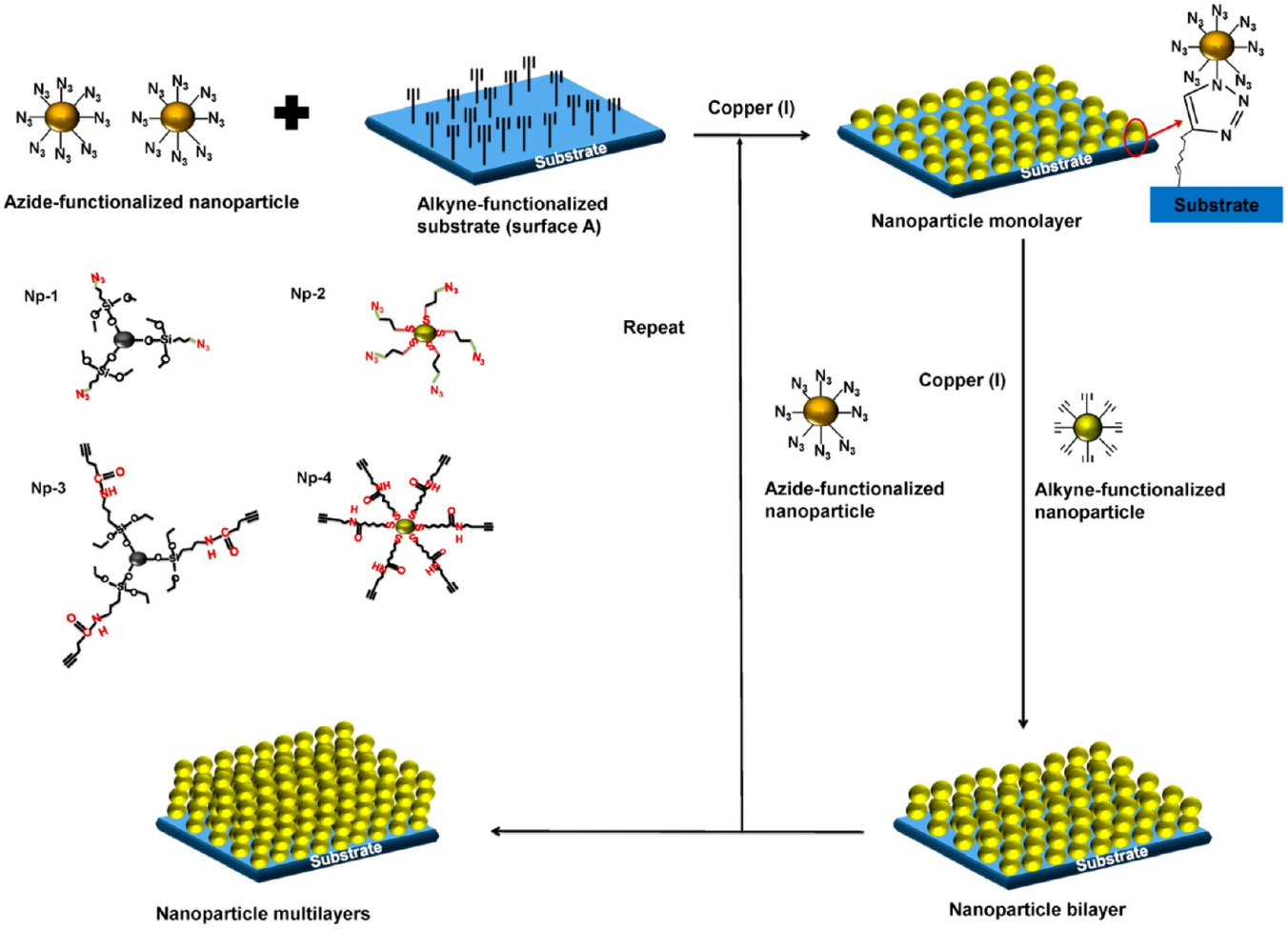

utilization of the copper(I)-catalyzed azide−alkyne cycloaddition (CuAAC) click reaction[34,35] for fabricating heterostructures offers a number of advantages as a chemical approach: (1) the triazole linkage between the click moieties offers high stability, even under highly oxidizing conditions, and supports electron transfer,[36−39] (2) it offers the ability to modify electrodes at room temperature and circumvent the problem of aggregation associated with the thermal processing of nanoparticles, (3) it is scalable to large areas, and (4) it provides flexibility and control in the formation of multilayers of differing metallic-semiconductor nanoparticles, enabling versatile heterostructure fabrication.

To demonstrate the generality of the method and the possible heterostructures, we have fabricated both monolayer and tailored multilayers of metallic, semiconducting, and dielectric nanoparticles on different semiconductor surfaces (e.g., silicon, indium tin oxide (ITO), stainless steel, and titania) via copper(I)-catalyzed azide−alkyne cycloaddition (CuAAC) click reaction. Heterostructures should be active for surface electrochemistry and stable under external potentials or potentials generated because of the absorption of solar radiation. To demonstrate these issues, we have tested the activity of these heterostructures as model systems for electrochemical water splitting, methanol oxidation, and photocatalytic degradation of Rhodamine B (RhB) dye. We observed that the electrochemical interfaces exhibit high stability for 150 electrochemical cycles, which is attributed to the strong triazole linkage between the metallic and semiconductor surfaces. Furthermore, we have tested the stability at a constant potential (0.75 V vs SCE) and different electrolyte pH (both acidic and basic medium) for 6 h and observed an insignificant decrease in the current density. These results suggest a path to design metallic-semiconductor heterostructures, to perform electrochemical reactions, and to interact with a large fraction of the solar spectrum. We have also fabricated tailored multilayered heterostructures using various nanoparticles (including gold, gold@TiO_2, silica, gold@silica) on different substrates (silicon, titania, ITO, stainless steel) to support further the generality and applicability of the approach to fabricating hybrid heterostructures of different metallic-semiconductor nanoparticles.

RESULTS AND DISCUSSION

Scheme 1 shows a schematic representation of the fabrication of tailored monolayers and multilayers of nanoparticles onto alkyne-functionalized substrates (e.g., silicon, glass, titania, ITO, and stainless steel) using click-chemistry-mediated, layer-by-layer (LbL) assembly. The substrates and nanoparticles were surface modified with alkyne and azide functionality, respectively (see the Supporting Information). Alkyne-functionalized substrates (surface A) were immersed in a 3.5 wt % solution of azide-functionalized nanoparticles (**Np-1**/**Np-**

dx.doi.org/10.1021/am402398h | ACS Appl. Mater. Interfaces 2013, 5, 9554−9562

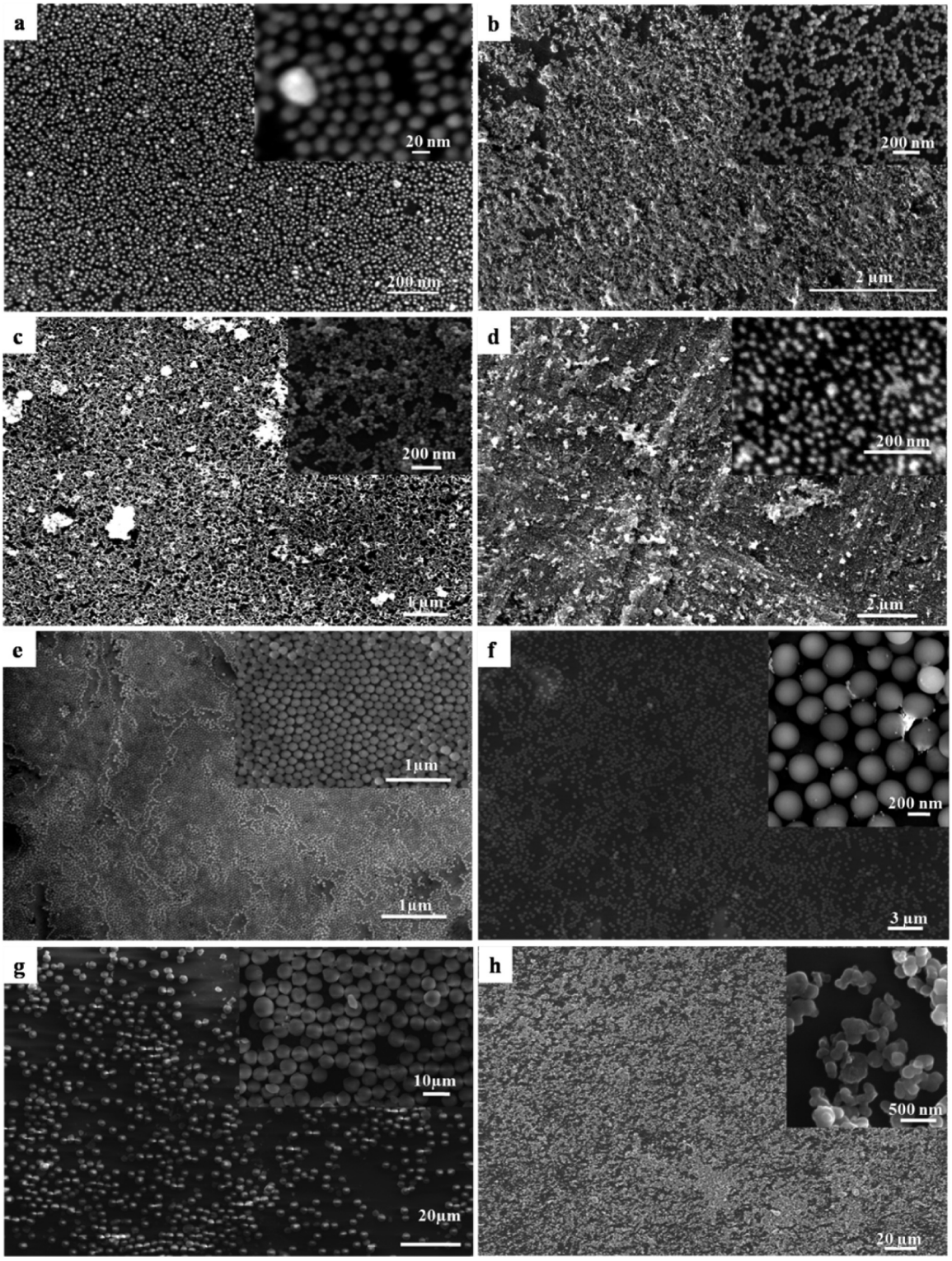

Figure 1. SEM images of a monolayer of azide-functionalized gold nanoparticles on alkyne-functionalized substrates of (a) silicon, (b) ITO, (c) titania, and (d) stainless steel. SEM images of monolayers of (e) 0.1 μm and (g) 5 μm azide-functionalized silica nanoparticle monolayers on alkyne-functionalized silicon substrate, (f) a monolayer of 0.33 μm azide-functionalized silica nanoparticles on an alkyne-functionalized glass substrate, and (h) a monolayer of alkyne-functionalized TiO_2 nanoparticles on an azide-functionalized silicon substrate.

2) in tetrahydrofuran (THF) for 12 h and then immersed in an aqueous solution of copper sulfate (10 mM) and ascorbic acid (50 mM) for another 6 h to catalyze the click reaction. Next, the substrates were washed three times with acetone followed by sonication for 30 min in THF to remove any physically attached nanoparticles. In the next step, the monolayer@substrate was immersed in an alkyne-functionalized nanoparticle (**Np-3**/**Np-4**) solution to form a bilayer. This process is repeated to form the tailored multilayers of nanoparticles on the desired substrates. To prove the generality and versatility of

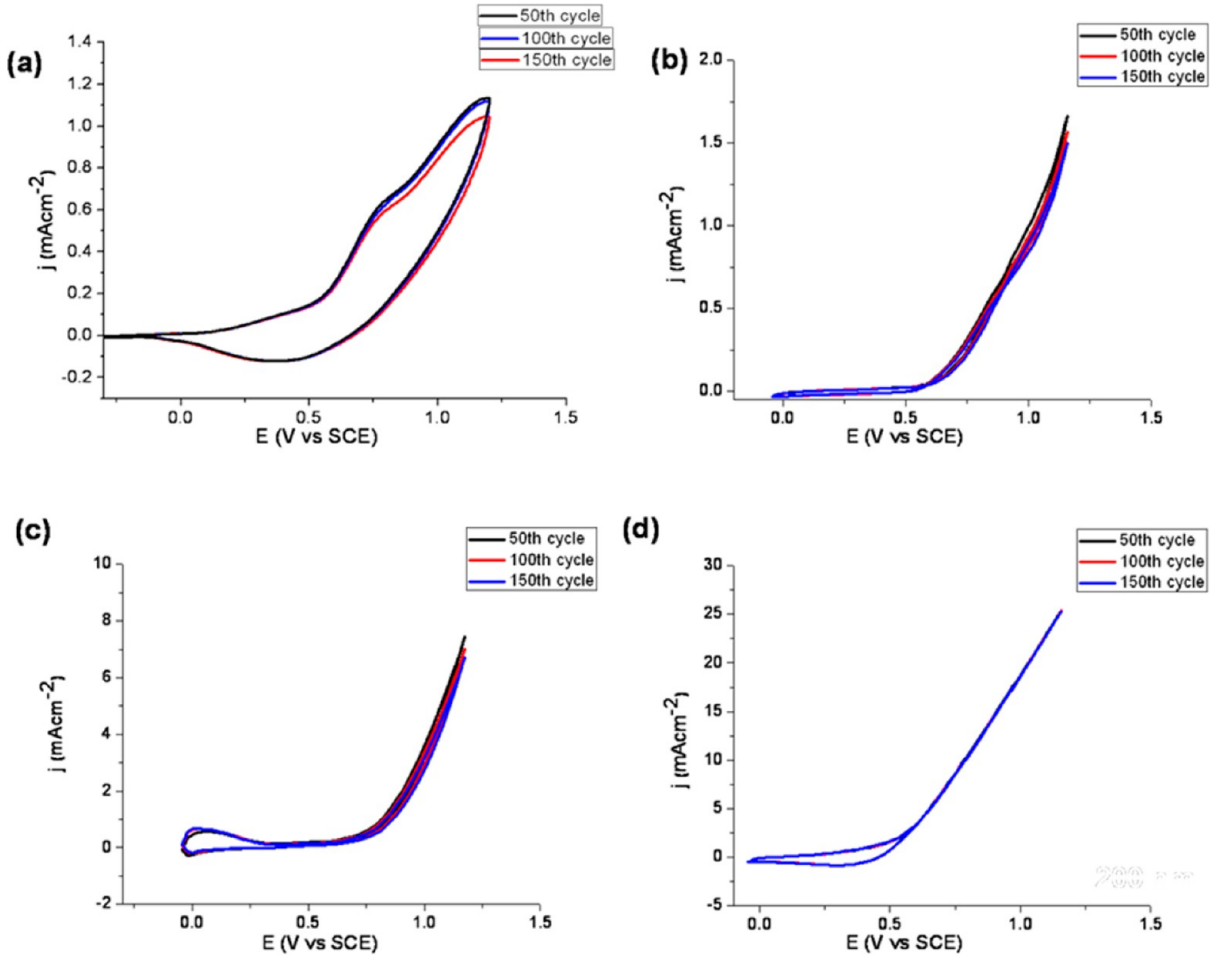

Figure 2. Cyclic voltammetric results for the analysis of the stability of (a) Au@silicon, (b) Au@titania, (c) Au@ITO, and (d) Au@stainless steel substrates.

the proposed approach, we have fabricated monolayers and tailored multilayers of gold and silica nanoparticles over a variety of substrates, such as silicon, glass, titania, ITO, and stainless steel. Additionally, we have extended the proposed approach to attaching a monolayer of alkyne-functionalized nanoparticles (**Np-3**/**Np-4**) onto azide-functionalized substrates (Scheme S1), which further supports the generality and versatility of the proposed approach.

The nanoparticles and substrates were characterized after the surface modification with click moieties (alkyne/azide) using FTIR and contact-angle measurements. The FTIR spectra of azide-functionalized silica (**Np-1**, Figure S1) and gold nanoparticles (**Np-2**, Figure S2) show peaks at ~2110 cm^{-1} that confirm the presence of azide groups on the nanoparticles. Figures S3–S5 show peaks at ~2250 cm^{-1}, which confirm the presence of alkyne groups on the surfaces of the silica, TiO_2 (**Np-3**), and gold nanoparticles (**Np-4**). Additionally, an increase in the contact-angle measurements on the alkyne-functionalized substrates (silicon (Θ_a ~97.8 ± 2°), titania (Θ_a ~104.5 ± 2°), ITO (Θ_a ~104 ± 2°), and stainless steel (Θ_a ~93.8 ± 2°)) compared to the bare substrates supports the formation of hydrophobic monolayers of terminal alkynes (Figure S6).[40−42] The relatively high contact angle for Ti and ITO versus Si and stainless steel suggests a higher density of 'click' groups on the surface.

Monolayer of Nanoparticles on Substrates. Scanning electron microscopy (SEM) images in Figure 1 clearly show the formation of monolayers of gold, TiO_2, and silica nanoparticles on a variety of substrates, as described in Scheme 1. Figure 1 panels a and e–g shows densely packed monolayers of azide-functionalized gold (~ 20 nm) and silica nanoparticles (~ 0.1 μm, 0.33 μm, 5 μm) on alkyne-functionalized silicon wafers, respectively. Figure 1b–d shows monolayers of azide-functionalized gold nanoparticles (~ 20 nm) on alkyne-functionalized ITO, titania, and stainless steel substrates, respectively. This result clearly shows that the proposed approach can be applied to the fabrication of monolayers of different sized nanoparticles over large areas of various substrates with minimal aggregation. However, it is clear from Figure 1 that increases in the size of the particles results in more open spaces within the hexagonal closed packed monolayers on the same substrates. A study[45] has explored the effects of particle volume fraction, particle size, and particle-substrate and particle-particle interactions on the growth rate of nanoparticle assemblies. From this study, an empirical relationship between the above-mentioned factors for nanoparticle monolayers is given by the following equation

$$g = \frac{\alpha j_e \emptyset}{0.605 d(1 - \emptyset)}$$

where g is the growth rate of the nanoparticle monolayer, α is a constant whose value depends on the particle-particle and particle-substrate interactions, Ø is the particle volume fraction, and d is the diameter of particles. It is clear from the above

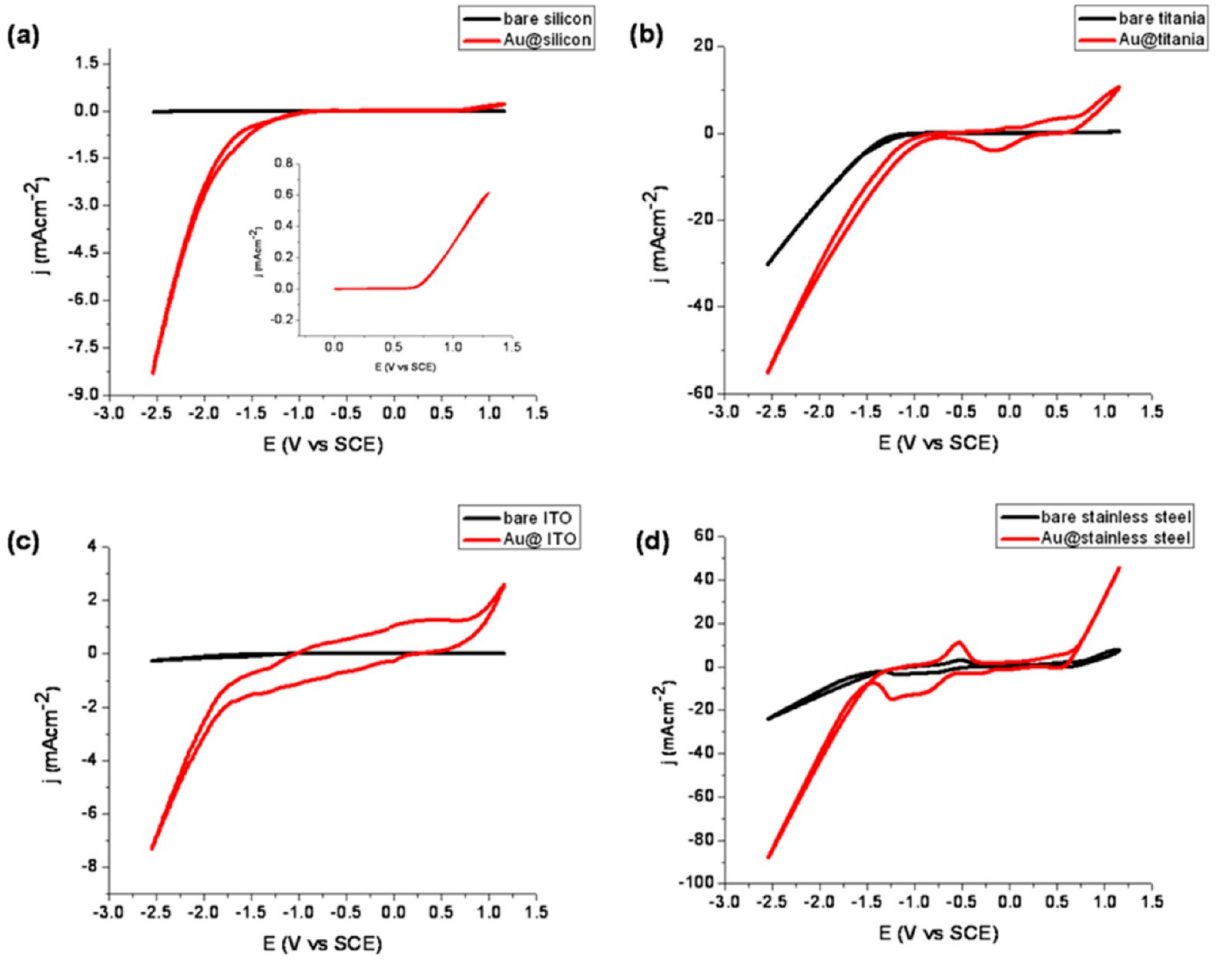

Figure 3. Cyclic voltammetric results for water splitting on (a) Au@silicon, (b) Au@titania, (c) Au@ITO, and (d) Au@stainless steel substrates.

equation that the growth rate of the particle monolayer assemblies varies inversely with the particle size.[45]

We note that titania and stainless steel possess a higher density of nanoparticles compared to the silicon and ITO substrates. Qualitatively, we can attribute the particle density to a convolution of the following factors: (1) the density of click groups present on the substrate surface, which in turn depends on the surface chemistry of the substrates, (2) surface roughness created as a result of the pretreatment of the substrates, and (3) solvent interaction with the substrate/nanoparticles. After the alkyne modifications, the contact angle of a titania/indium tin oxide (ITO) substrate is ∼104° and that of silicon/stainless steel is ∼96°, thereby indicating the greater hydrophobicity of the alkyne-modified titania/indium tin oxide (ITO) substrate. This difference in hydrophobicity can be correlated to the difference in the densities of alkyne groups on the substrates. We attribute the higher density of particles on the titania substrate to the presence of the alkyne groups. To qualitatively estimate the increase in surface roughness following the piranha wash, we kept track of the color change in the pretreatment solution. We interpreted a greater color change in the pretreatment solution as a greater removal of the substrate because of the piranha wash. We observed that the color change was greatest with stainless steel. On the basis of this qualitative measure, we attributed the greater particle density on stainless steel (Figure 1d) to the greater surface roughness following the piranha wash.

Substrate-solvent interactions and particle-solvent interactions also play an important role in controlling the density of the nanoparticles. To study the effect of these interactions, we performed additional experiments with alkyne-functionalized silicon substrates and azide-functionalized gold nanoparticles dispersed in different solvents, such as dimethylsulfoxide and dichloromethane, while keeping all the reaction conditions similar (Figure S7). We observed that these solvents led to greater aggregation of gold nanoparticles assembled on silicon substrates than when tetrahydrofuran was used as a solvent (Figure 1a). Although this observation does not make a more microscopic connection between the molecular nature of the solvent and the aggregation of the particles, the observation clearly suggests that the nature of the solvent plays a critical role in the assembly of the particles. Additional aspects correlating the nature of the solvent-substrate interactions to the assembly of nanoparticles are mentioned by a few reports.[43,44]

To obtain the hexagonal close packing of nanoparticles, we performed experiments with different concentrations of silica nanoparticles (i.e., 1, 1.5, 2, and 3.5 wt %). SEM images (Figure S8) clearly suggest that monolayers formed from the 1, 1.5, and 2.5 wt % nanoparticle concentrations had a lower density of nanoparticles than those from the 3.5 wt % (Figure 1e). This result suggests that the trends in density can be correlated to the concentration of the nanoparticles. Furthermore, we anticipate that the maximum density of nanoparticles is

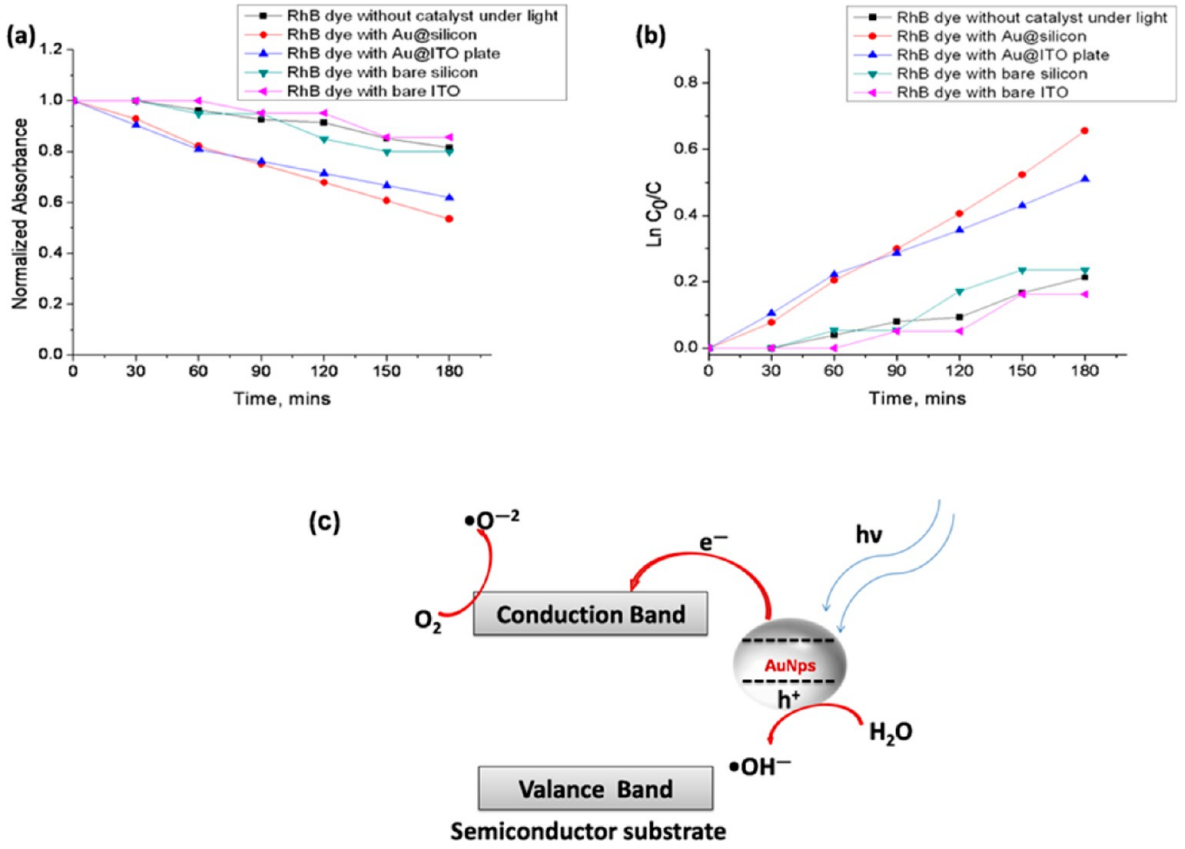

Figure 4. (a) Absorbance vs time curve for RhB dye under light illumination, (b) rate constant curves for RhB dye degradation, and (c) schematic diagram for the proposed dye-degradation mechanism.

attained when the hexagonal close-packed structure is achieved (Figure 1e).

Additionally, as described in Scheme S1, monolayers of alkyne-functionalized TiO_2 nanoparticles (size ~200 nm, Figure 1h), gold nanoparticles (size ~10 nm, Figure S9a), and silica nanoparticles (size ~120 nm, Figure S9b) have also been fabricated on azide-functionalized silicon substrates, which supports the generality of the proposed approach for the fabrication of a variety of nano/heterostructures. Furthermore, the FTIR peak at 1600 cm^{-1} confirms the triazole linkage between the click moieties present on the particles and substrates (Figure S10).

Electrochemical Methanol Oxidation and Water Splitting. *Methanol Oxidation.* Figure 2 shows the cyclic voltammetric profiles of the gold-nanoparticle monolayers (~8 nmoles per cm^2) on different substrates (Au@silicon (Figure 2a), Au@titania (Figure 2b), Au@ITO (Figure 2c), Au@SS (Figure 2d)), showing the stability of the electrolyte solution (0.1 M NaOH + 2.5 M MeOH) at a 500 mV/s scan rate. The potential range has been restricted in all four cases (i.e., Au@silicon substrate, Au@titania substrate, Au@ITO substrate, and Au@stainless steel substrates) to 1.2 V (all potentials are measured vs Ag/AgCl and are expressed vs SCE) to prevent the electrochemical oxidation of gold that occurs at potentials beyond 1.3 V. In the alkaline solutions, the oxidation current arises because of methanol oxidation followed by oxygen evolution.[46] The oxidation of methanol is initiated by the deprotonation of the C atom, resulting in C_xH_2OH radical bound to the gold surface (x represents a valence bond with the gold surface).[8,47]At potentials below 0.7 V, the methanol oxidation proceeds via the dissociation of a C−H bond in the methanol as opposed to a O−H bond at higher potentials. It has been shown that at potentials above 0.7 V, both OH^- and CH_3OH are adsorbed on the active surface sites until OH^- reaches a maximum.[8,46,48] Once this maximum is attained, the current stabilizes, and the reaction proceeds via the formation of the methoxy radical.[8,48,49] From the cyclic voltammetry curves (Figure 2), the high stability of the gold-nanoparticle monolayers on different substrates can be attributed to the triazole linkage between the click moieties, which firmly anchored the gold nanoparticles onto the semiconductor surface (Figure S11). This result is further confirmed by the FTIR peak at approximately 1600 cm^{-1}, indicating the presence of triazole linkages between the gold nanoparticles and the substrate after 150 cycles (Figure S12). However, a slight decrease in the current density (approximately 15%) by 150 cycles for Au@titania and Au@ITO (Figure 2b,c) was observed, likely because of either the instability of the conducting layers (ITO) or the oxidation of substrates (titania).[36]

Water Splitting. Furthermore, we examined gold nanoparticle monolayers (~8 nmoles per cm^2) on different substrates (i.e., silicon, ITO, titania, and stainless steel) for electrochemical water splitting. Figure 3 shows cyclic voltammetric profiles in a 0.1 M NaOH electrolyte solution. The onset potential at approximately 0.7 V (vs SCE) for all four samples shows the oxygen-evolution current at approximately 0.6, 11, 2.3, and 45 mA/cm^2 for the gold-nanoparticle monolayers on silicon, titania, ITO, and stainless steel substrates, respectively, which is higher than that of the bare substrates. The overall current density will be dependent on three essential factors: (1) the density of the nanoparticles, (2)

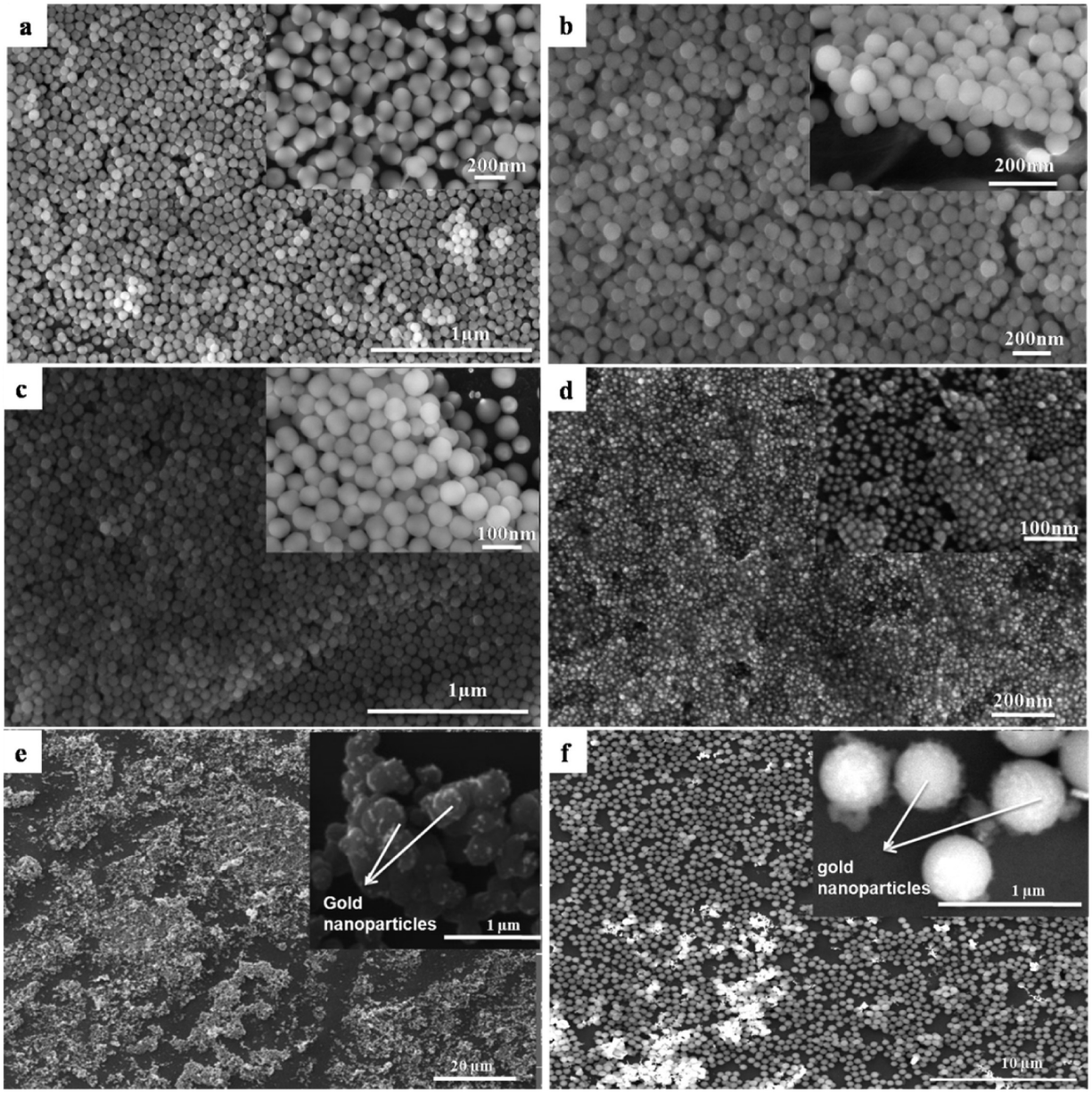

Figure 5. SEM images of (a) two, (b) three, and (c) four layers of silica nanoparticles and (d) bilayer of gold nanoparticles, (e) gold@TiO_2@silicon, and (f) gold@SiO_2@silicon.

the electrocatalytic activity of the substrate, and (3) the metal-nanoparticle support interactions. The first two factors are more easily calibrated. Both the density of the nanoparticles and the electrochemical activity of the substrate favor higher current density in the gold-nanoparticle assembly on stainless steel. It should be mentioned that the overall current density observed in the gold-nanoparticle assembly on the substrate is not just a linear addition of contributions to the electrochemical reactivity from the gold and the substrate, indicating significant metal-support interactions.

The onset potential around −1.0 V (vs SCE) for Au@silicon, Au@titania, Au@ITO, and Au@stainless steel during reverse scan shows the hydrogen-evolution reaction. We observed a large amount of hydrogen-bubble evolution (starting at a potential of −1.0 V) and oxygen-bubble evolution (starting at a potential 0.7 V) from a 1 × 2 cm^2 gold-nanoparticle monolayer on stainless steel substrates immersed in a 0.1 M NaOH electrolyte solution.

To study the effect of the metal-semiconductor interface, an electrochemical water-splitting control experiment was performed under the same conditions as above with a sputtered thin film of gold (thickness ∼20 nm, detailed in the experimental conditions given in the Supporting Information) on the semiconductor surfaces. In the voltammetry experiment, a lower current density was observed for the gold thin film on semiconductor surfaces (silicon, ITO, titania, and stainless steel), as shown in Figure S13 in the Supporting Information. The lower current density can be attributed to the absence of porosity in the case of sputtered gold, which does not allow the electrolyte to access the interfacial sites (Figure S13). This fact lends credence to the efficiency of the proposed approach for performing chemical reactions. We note that the current density is higher in the case of a gold thin film on a silicon

substrate than a gold-nanoparticle monolayer on a silicon substrate. This effect may be attributed to a lower coverage of gold nanoparticles on the silicon substrate than the thin film.

We performed an additional control experiment to prepare nanoparticle assemblies by spin-coating gold nanoparticles onto a silicon substrate (1000 rpm for 45 sec). An electrochemical water-splitting experiment was performed under an identical range of pH (0.1 M NaOH) and other operating conditions. The cyclic voltammetric analysis clearly shows a significant decrease in the current density from 120 to 70 μA (Figure S14a) within five cycles, and this decrease can be correlated to the loss of nanoparticles during the electrochemical reaction, which we calibrate using SEM images before (Figure S14b) and after the electrochemical reaction (Figure S14c). This observation further supports the viewpoint that the lack of covalent linkages results in a nanoparticle assembly with a lower stability.

Photocatalytic RhB Dye Degradation. To examine the photocatalytic activity of gold-nanoparticle monolayers bound to different substrates via click chemistry, we studied the photochemical degradation of a Rhodamine B (RhB) dye solution in neutral aqueous medium (Figure 4). Figure 4a shows the absorbance at 553 nm versus time curve for an RhB dye solution in contact with the different samples. The decrease in the absorbance peak at 553 nm with time (Figure S15) suggests a faster degradation of the RhB dye in the presence of Au@silicon and Au@ITO than under illumination without the catalyst. Au@silicon shows better catalytic activity (48% degradation efficiency) compared to Au@ITO (40% degradation), which may be because of the single-crystalline nature of silicon and silicon itself absorbs light. In addition to the gold nanoparticles, these features further help to improve the efficiency. A plot of ln C_0/C(where C_0 is the initial concentration of the dye and C is the concentration of the dye at different time intervals) versus time is shown in Figure 4b, clearly suggesting that in the presence of gold-nanoparticle monolayer samples RhB dye degradation follows pseudo-first-order reaction kinetics. The calculated pseudo-first-order rate constants in the presence of Au@silicon and Au@ITO were found to be 0.003 and 0.002 min^{-1}, respectively, which are high compared to the control samples. We also note that the control samples did not follow pseudo-first-order degradation, and under dark conditions with and without using the prepared catalysts there was almost no change in the absorbance peak intensity for almost 120 min (Figure S16).

Figure 4c shows a schematic representation of a possible mechanism for the degradation of RhB dyes. During the photocatalytic degradation of the RhB dye, both the SPR effect of the gold nanoparticles and the electronic transition in the gold nanoparticles play roles (Figure 4c). Upon illumination, the gold nanoparticles absorb resonant photons and excite electrons from the band below the Fermi level to higher energy states. The excited electrons are transferred to the conduction band of the semiconductors, where the electrons are further transferred to adsorbed O_2 molecules to generate $\bullet O^{-2}$ species. Simultaneously, photogenerated holes react with water molecules to generate hydroxyl ($\bullet OH^-$) radicals, which are mainly responsible for the degradation of the RhB dye. Therefore, we believe that the SPR effect cannot be decoupled from the electronic transitions, and both play significant roles in RhB dye degradation.[4,15,50,51]

Hybrid Multilayer Heterostructures. Heterostructures with alternative layers of different metal and semiconductor nanoparticles can provide a path to fabricate hybrid structures of different band-gap semiconductor materials, which can be useful for capturing a large fraction of the solar spectrum. To explore the applicability of the proposed approach for the design of such hybrid heterostructures, we have shown controlled, multilayer formation of silica nanoparticles, gold-TiO_2 multilayer heterostructures, and gold-coated silica nanoparticle heterostructures. To prove the concept of tailored multilayers, we have chosen silica nanoparticles for characterization purposes. Figure 5 shows tailored multilayers of different nanoparticles fabricated by sequential deposition (LbL) of alkyne/azide-functionalized nanoparticles on freely available azide/alkyne moieties on nanoparticle monolayers. Figure 5a–c show SEM images of two, three, and four tailored multilayers of silica nanoparticles on alkyne-functionalized silicon substrates, respectively. Tailored multilayers of silica nanoparticles show dense packing and regions that have hcp structure, which clearly suggests that this approach can be utilized to prepare tailored multilayers of materials with different band gaps and electrochemical and photoelectrochemical properties. Additionally, Figure 5d shows a bilayer of gold nanoparticles on an alkyne-functionalized silicon substrate with minimal aggregation, which further supports the generality and versatility of the proposed approach. Additionally, an azide-functionalized gold bilayer on an alkyne-functionalized TiO_2 monolayer (Figure 5e) and azide-functionalized gold-coated silica nanoparticle (size ~550 nm, Figure 5f, also see the Supporting Information) monolayers on an azide-functionalized silicon substrate have been fabricated, as described in Scheme S1. The above SEM results clearly show that the proposed approach allows for the assembly of a variety of nanoparticles in controlled hybrid multilayer heterostructures.

CONCLUSIONS

Our results demonstrate a generic approach for processing metallic mono/tailored multilayers on a variety of substrates (silicon, titania, ITO, and stainless steel) via click chemistry. We observed an enhancement in the electro/photocatalytic activity and stability of heterostructures towards electrochemical methanol oxidation, electrochemical water splitting, and photocatalytic degradation of RhB dye. The enhancement in the stability of the heterostructures is because of the stable triazole linkage formed between the azide and alkyne groups present on the gold nanoparticles and substrates surfaces, respectively. Additionally, hybrid tailored mono/multilayer heterostructures of gold, TiO_2, and silica nanoparticles on silicon and glass substrates support the generality of the proposed approach and illustrate a methodology for designing stable hybrid heterostructures that can interact with a large fraction of the solar spectrum.

ASSOCIATED CONTENT

Supporting Information

Experimental procedures, characterization techniques, SEM images, FTIR spectroscopy, water contact-angle measurements, UV–vis absorption spectra, and cyclic voltammetry analysis of control samples. This material is available free of charge via the Internet at http://pubs.acs.org.

AUTHOR INFORMATION

Corresponding Authors

*E-mail: rragan@uci.edu (R.R.).
*E-mail: rpala@iitk.ac.in (R.G.S.P.).

*E-mail: srisiva@iitk.ac.in (S.S.).

Notes

The authors declare no competing financial interest.

■ ACKNOWLEDGMENTS

We acknowledge Tatsat Banerjee for help with the multilayer experiments. We gratefully acknowledge the support from the Indo-US Science and Technology Forum and the Technology System Development program, Department of Science and Technology, Government of India via project DST/ME/20110310.

■ REFERENCES

(1) Asahi, R.; Morikawa, T.; Ohwaki, T.; Aoki, K.; Taga, Y. *Science* **2001**, *293*, 269−271.
(2) Atwater, H. A.; Polman, A. *Nat. Mater.* **2010**, *9*, 205−213.
(3) Chen, X. B.; Shen, S. H.; Guo, L. J.; Mao, S. S. *Chem. Rev.* **2010**, *110*, 6503−6570.
(4) Linic, S.; Christopher, P.; Ingram, D. B. *Nat. Mater.* **2011**, *10*, 911−921.
(5) Reece, S. Y.; Hamel, J. A.; Sung, K.; Jarvi, T. D.; Esswein, A. J.; Pijpers, J. J. H.; Nocera, D. G. *Science* **2011**, *334*, 645−648.
(6) Christopher, P.; Xin, H. L.; Linic, S. *Nat. Chem.* **2011**, *3*, 467−472.
(7) Lee, I.; Joo, J. B.; Yin, Y. D.; Zaera, F. *Angew. Chem., Int. Ed.* **2011**, *50*, 10208−10211.
(8) Rodriguez, P.; Kwon, Y.; Koper, M. T. M. *Nat. Chem.* **2011**, *4*, 177−182.
(9) Linsebigler, A. L.; Lu, G. Q.; Yates, J. T. *Chem. Rev.* **1995**, *95*, 735−758.
(10) Hu, Y. S.; Kleiman-Shwarsctein, A.; Forman, A. J.; Hazen, D.; Park, J. N.; McFarland, E. W. *Chem. Mater.* **2008**, *20*, 3803−3805.
(11) Kleiman-Shwarsctein, A.; Hu, Y. S.; Forman, A. J.; Stucky, G. D.; McFarland, E. W. *J. Phys. Chem. C* **2008**, *112*, 15900−15907.
(12) Xu, W.; Jain, P. K.; Beberwyck, B. J.; Alivisatos, A. P. *J. Am. Chem. Soc.* **2012**, *134*, 3946−3949.
(13) Christopher, P.; Ingram, D. B.; Linic, S. *J. Phys. Chem. C* **2010**, *114*, 9173−9177.
(14) Christopher, P.; Xin, H. L.; Marimuthu, A.; Linic, S. *Nat. Mater.* **2012**, *11*, 1044−1050.
(15) Ingram, D. B.; Christopher, P.; Bauer, J. L.; Linic, S. *ACS Catal.* **2011**, *1*, 1441−1447.
(16) Ingram, D. B.; Linic, S. *J. Am. Chem. Soc.* **2011**, *133*, 5202−5205.
(17) Tang, M. L.; Grauer, D. C.; Lassalle-Kaiser, B.; Yachandra, V. K.; Amirav, L.; Long, J. R.; Yano, J.; Alivisatos, A. P. *Angew. Chem., Int. Ed.* **2011**, *50*, 10203−10207.
(18) Chiarello, G. L.; Selli, E.; Forni, L. *Appl. Catal., B* **2008**, *84*, 332−339.
(19) Hou, Y. D.; Abrams, B. L.; Vesborg, P. C. K.; Bjorketun, M. E.; Herbst, K.; Bech, L.; Setti, A. M.; Damsgaard, C. D.; Pedersen, T.; Hansen, O.; Rossmeisl, J.; Dahl, S.; Norskov, J. K.; Chorkendorff, I. *Nat. Mater.* **2011**, *10*, 434−438.
(20) Ke, D. N.; Peng, T. Y.; Ma, L.; Cai, P.; Jiang, P. *Appl. Catal., A* **2008**, *350*, 111−117.
(21) Liu, Z. W.; Hou, W. B.; Pavaskar, P.; Aykol, M.; Cronin, S. B. *Nano Lett.* **2011**, *11*, 1111−1116.
(22) Zhang, Q.; Lima, D. Q.; Lee, I.; Zaera, F.; Chi, M. F.; Yin, Y. D. *Angew. Chem., Int. Ed.* **2011**, *50*, 7088−7092.
(23) Rivest, J. B.; Swisher, S. L.; Fong, L. K.; Zheng, H. M.; Alivisatos, A. P. *ACS Nano* **2011**, *5*, 3811−3816.
(24) Grzelczak, M.; Vermant, J.; Furst, E. M.; Liz-Marzan, L. M. *ACS Nano* **2010**, *4*, 3591−3605.
(25) Harfenist, S. A.; Wang, Z. L.; Alvarez, M. M.; Vezmar, I.; Whetten, R. L. *J. Phys. Chem.* **1996**, *100*, 13904−13910.
(26) Hurst, K. M.; Ansari, N.; Roberts, C. B.; Ashurst, W. R. *J. Microelectromech. Syst.* **2011**, *20*, 424−435.
(27) Kane, J.; Inan, M.; Saraf, R. F. *ACS Nano* **2010**, *4*, 317−323.
(28) Maury, P. A.; Reinhoudt, D. N.; Huskens, J. *Curr. Opin. Colloid Interface Sci.* **2008**, *13*, 74−80.
(29) McCarty, L. S.; Winkleman, A.; Whitesides, G. M. *Angew. Chem., Int. Ed.* **2007**, *46*, 206−209.
(30) Jiang, P.; McFarland, M. J. *J. Am. Chem. Soc.* **2004**, *126*, 13778−13786.
(31) Huang, S. J.; Tsutsui, G.; Sakaue, H.; Shingubara, S.; Takahagi, T. *J. Vac. Sci. Technol., B* **2001**, *19*, 2045−2049.
(32) Yang, H. T.; Jiang, P. *Langmuir* **2010**, *26*, 13173−13182.
(33) Awazu, K.; Fujimaki, M.; Rockstuhl, C.; Tominaga, J.; Murakami, H.; Ohki, Y.; Yoshida, N.; Watanabe, T. *J. Am. Chem. Soc.* **2008**, *130*, 1676−1680.
(34) Kolb, H. C.; Finn, M. G.; Sharpless, K. B. *Angew. Chem., Int. Ed.* **2001**, *40*, 2004−2021.
(35) Rostovtsev, V. V.; Green, L. G.; Fokin, V. V.; Sharpless, K. B. *Angew. Chem., Int. Ed.* **2002**, *41*, 2596−2599.
(36) Benson, M. C.; Ruther, R. E.; Gerken, J. B.; Rigsby, M. L.; Bishop, L. M.; Tan, Y. Z.; Stahl, S. S.; Hamers, R. J. *ACS Appl. Mater. Interfaces* **2011**, *3*, 3110−3119.
(37) Cardiel, A. C.; Benson, M. C.; Bishop, L. M.; Louis, K. M.; Yeager, J. C.; Tan, Y. Z.; Hamers, R. J. *ACS Nano* **2012**, *6*, 310−318.
(38) Collman, J. P.; Devaraj, N. K.; Chidsey, C. E. D. *Langmuir* **2004**, *20*, 1051−1053.
(39) Devaraj, N. K.; Decreau, R. A.; Ebina, W.; Collman, J. P.; Chidsey, C. E. D. *J. Phys. Chem. B* **2006**, *110*, 15955−15962.
(40) Ciampi, S.; Bocking, T.; Kilian, K. A.; James, M.; Harper, J. B.; Gooding, J. J. *Langmuir* **2007**, *23*, 9320−9329.
(41) Flink, S.; van Veggel, F.; Reinhoudt, D. N. *J. Phys. Org. Chem.* **2001**, *14*, 407−415.
(42) Sieval, A. B.; Demirel, A. L.; Nissink, J. W. M.; Linford, M. R.; van der Maas, J. H.; de Jeu, W. H.; Zuilhof, H.; Sudholter, E. J. R. *Langmuir* **1998**, *14*, 1759−1768.
(43) Laskar, I. R.; Watanabe, S.; Hada, M.; Yoshida, H.; Li, J.; Iyoda, T. *Surf. Sci.* **2009**, *603*, 625−631.
(44) Muralidharan, G.; Sivaraman, S. K.; Santhanam, V. *Nanoscale* **2011**, *3*, 2138−2141.
(45) Dimitrov, A. S.; Nagayama, K. *Langmuir* **1996**, *12*, 1303−1311.
(46) Ballarin, B.; Cassani, M. C.; Scavetta, E.; Tonelli, D. *Electrochim. Acta* **2008**, *53*, 8034−8044.
(47) Matsuoka, K.; Miyazaki, K.; Iriyama, Y.; Kikuchi, K.; Abe, T.; Ogumi, Z. *J. Phys. Chem. C* **2007**, *111*, 3171−3174.
(48) Iwasita, T. *Electrochim. Acta* **2002**, *48*, 289−289.
(49) Hernandez, J.; Solla-Gullon, J.; Herrero, E.; Aldaz, A.; Feliu, J. M. *Electrochim. Acta* **2006**, *52*, 1662−1669.
(50) Wang, P.; Huang, B. B.; Dai, Y.; Whangbo, M. H. *Phys. Chem. Chem. Phys.* **2012**, *14*, 9813−9825.
(51) Wang, P.; Huang, B. B.; Qin, X. Y.; Zhang, X. Y.; Dai, Y.; Wei, J. Y.; Whangbo, M. H. *Angew. Chem., Int. Ed.* **2008**, *47*, 7931−7933.